Near-infrared spectral mapping of Titan's mountains and channels

Jason Barnes, Jani Radebaugh, Robert Brown, Steve Wall, Laurence Soderblom, Jonathan Lunine, Devon Burr, Christophe Sotin, Stéphane Le Mouélic, Sebastien Rodriguez, et al.

JOURNAL OF GEOPHYSICAL RESEARCH, VOL. 112, E11006, doi:10.1029/2007JE002932, 2007

Near-infrared spectral mapping of Titan's mountains and channels

Jason W. Barnes,[1,2] Jani Radebaugh,[3] Robert H. Brown,[2] Steve Wall,[4] Laurence Soderblom,[5] Jonathan Lunine,[2] Devon Burr,[6] Christophe Sotin,[7] Stephane Le Mouélic,[7] Sebastien Rodriguez,[8] Bonnie J. Buratti,[4] Roger Clark,[9] Kevin H. Baines,[4] Ralf Jaumann,[10] Phillip D. Nicholson,[11] Randolph L. Kirk,[5] Rosaly Lopes,[4] Ralph D. Lorenz,[12] Karl Mitchell,[4] and Charles A. Wood[13]

Received 1 May 2007; revised 26 July 2007; accepted 28 August 2007; published 20 November 2007.

[1] We investigate the spectral reflectance properties of channels and mountain ranges on Titan using data from Cassini's Visual and Infrared Mapping Spectrometer (VIMS) obtained during the T9 encounter (26 December 2005). We identify the location of channels and mountains using synthetic aperture radar maps obtained from Cassini's RADAR instrument during the T13 (30 April 2006) flyby. Channels are evident even in VIMS imaging with spatial resolution coarser than the channel size. The channels share spectral characteristics with Titan's dark blue terrain (e.g., the Huygens landing site) that is consistent with an enhancement in water ice content relative to the rest of Titan. We use this fact to measure widths of ~1 km for the largest channels. Comparison of the data sets shows that in our study area within the equatorial bright spectral unit east of Xanadu, mountains are darker and bluer than surrounding smooth terrain. These results are consistent with the equatorial bright terrain possessing a veneer of material that is thinner in the regions where there are mountains and streambeds that have likely undergone more recent and extensive erosion. We suggest a model for the geographic relationship of the dark blue, dark brown, and equatorial bright spectral units based on our findings.

Citation: Barnes, J. W., et al. (2007), Near-infrared spectral mapping of Titan's mountains and channels, *J. Geophys. Res.*, *112*, E11006, doi:10.1029/2007JE002932.

1. Introduction

[2] How the nature of Titan's surface relates to infrared reflectivity remains largely uncertain. Unambiguous identification of surface materials has proven challenging through Titan's narrow spectral windows, but the general spectral signature matches that of dirty water ice [e.g., *Griffith et al.*, 1991, 2003; *Coustenis et al.*, 1995; *McCord et al.*, 2006; *Negrão et al.*, 2006]. Titan's surface shows a high degree of spectral variability at the global scale as seen by Cassini's Visual and Infrared Mapping Spectrometer (VIMS) [*Barnes et al.*, 2005, 2007; *McCord et al.*, 2006], with some regions showing what has been interpreted as resulting from varying levels of water-ice content [*Rodriguez et al.*, 2006].

[3] Many different geological surface processes have been identified on the basis of morphology. Titan exhibits craters [*Elachi et al.*, 2006], sand dunes [*Lorenz et al.*, 2006], stream channels [*Tomasko et al.*, 2005; *Soderblom et al.*, 2007b], lakes [*Stofan et al.*, 2007], and various features of possible extrusive origin [*Sotin et al.*, 2005; *Barnes et al.*, 2006; *Lopes et al.*, 2007]. Recently Cassini has identified mountains estimated to be up to ~2 km in height [*Radebaugh et al.*, 2007; C. Sotin, VIMS reveals a moutain range on Titan, manuscript in preparation, 2007; hereinafter referred to as Sotin, manuscript in preparation, 2007]. The mountains are common and contiguous within the large bright region Xanadu (R. Kirk, RADAR observations from Cassini's T13 Titan flyby, manuscript in preparation, 2007; hereinafter referred to as Kirk, manuscript in preparation, 2007), and exist variously in small (~20–100km) clumps and linear chains [*Elachi et al.*, 2006; *Radebaugh et al.*, 2007; Sotin, manuscript in preparation, 2007; J. I. Lunine, Cassini RADAR's third and fourth looks at Titan, submitted to *Icarus*, 2007] elsewhere. The distribution of mountains so

[1]NASA Ames Research Center, Moffett Field, California, USA.
[2]Lunar and Planetary Laboratory, University of Arizona, Tucson, Arizona, USA.
[3]Department of Geological Sciences, Brigham Young University, Provo, Utah, USA.
[4]Jet Propulsion Laboratory, California Institute of Technology, Pasadena, California, USA.
[5]U.S. Geological Survey, Flagstaff, Arizona, USA.
[6]Carl Sagan Center, SETI Institute, Mountain View, California, USA.
[7]Laboratoire de Planétologie et Géodynamique, UMR CNRS, Universitéde Nantes, Nantes, France.
[8]Laboratoire AIM, Centre d'Étude de Saclay, DAPNIA/Sap, Centre de l'Orme des Merisiers, Gif sur Yvette, France.
[9]U.S. Geological Survey, Denver, Colorado, USA.
[10]DLR, Institute for Planetary Research, Berlin, Germany.
[11]Astronomy Department, Cornell University, Ithaca, New York, USA.
[12]Space Department, JHU Applied Physics Laboratory, Laurel, Maryland, USA.
[13]Planetary Science Institute, Tucson, Arizona, USA.

0148-0227/07/2007JE002932$09.00

far shows no obvious underlying structure but several different mechanisms for their formation have been hypothesized [*Radebaugh et al.*, 2007].

[4] The Descent Imager Spectral Radiometer (DISR) instrument on board the Huygens entry probe showed a complex array of hills, canyons, and channels at its landing site [*Tomasko et al.*, 2005; *Soderblom et al.*, 2007b]. The probe landed near a boundary between light and dark terrain as seen in both visible and near-infrared reflection [*Tomasko et al.*, 2005; *Rodriguez et al.*, 2006; *Soderblom et al.*, 2007a]. At the landing site, channels presumably carved by liquid methane were seen incised into bright terrain with relatively higher topography. The channels were no longer visible once they entered the lower, darker terrain [*Soderblom et al.*, 2007b]. The bright/dark dichotomy has been hypothesized [*Griffith et al.*, 1991; *Lunine*, 1992; *Smith et al.*, 1996] to be the result of dark, atmospheric-organic material settling uniformly onto the surface only to be washed toward and deposited into the lowlands (though it is not clear that such organic matter would be poorly reflective deep in the infrared as well as in the visible). This is consistent with areas with higher infrared reflectivities that, in general, stand topographically above those with lower infrared reflectivities, as is seen at the Huygens landing site [*Soderblom et al.*, 2007b].

[5] Channels have been observed from the Cassini orbiter by the RADAR [*Elachi et al.*, 2005], Imaging Science Subsystem (ISS) [*Porco et al.*, 2005], and VIMS [*Barnes et al.*, 2007] instruments. Though some channels are traceable for thousands of kilometers (R. D. Lorenz et al., Fluvial channels on Titan: Meteorological paradigm and Cassini RADAR observations, submitted to *Planetary and Space Science*, 2007; hereinafter referred to as Lorenz et al., submitted manuscript, 2007), others seen from the orbiter do not easily fit into a regional topographic framework (Kirk, manuscript in preparation, 2007); in some cases it is difficult to identify which direction is upstream and which is downstream. Benzene on Titan appears to be concentrated within channels and dark terrains (R. Clark et al., Detection of widespread aromatic and aliphatic hydrocarbon deposits on Titan, manuscript in preparation, 2007; hereinafter referred to as Clark et al., manuscript in preparation, 2007).

[6] In this paper we investigate the nature of Titan's mountains and channels using VIMS data in combination with RADAR data where appropriate. First we describe the data sets to be analyzed. Next we describe and investigate Titan's channels as seen with VIMS, and compare some of those channels directly with the same channels observed by RADAR. We then analyze the appearance and spectra of mountain ranges, and lastly we interpret the geophysical implications of the observed spectra and morphology.

2. Observations

2.1. VIMS

[7] The Visual and Infrared Mapping Spectrometer (VIMS) instrument on Cassini images at 352 wavelengths simultaneously using a spectral mapping technique [*Brown et al.*, 2004]. As VIMS operates between 0.3 μm and 5.1 μm, it is able to penetrate Titan's hazy atmosphere to observe the surface within the spectral windows at 0.83 μm, 0.94 μm, 1.08 μm, 1.28 μm, 1.6 μm, 2.0 μm, 2.7 μm, and 5.0 μm. Light scatter off of atmospheric haze particles at wavelengths shorter than 0.83 μm results in images dominated by bright, diffuse light that swamps the surface illumination. The scattered-light component affects VIMS' entire spectral range, but becomes progressively less important at longer wavelengths and is particularly low at 5.0 μm.

[8] Between the spectral windows listed above, absorption of light by various atmospheric gases prevents sunlight from reaching down to the surface and being scattered back to space. The wings of each spectral window are thus partially affected by absorption as well. The different relative intensities between windows are evidence for surface compositional variability, but unambiguous identification of surface composition requires the detection of discrete absorption features. Thus far discrete features have been found only within the 5.0μm window (Clark et al., manuscript in preparation, 2007; J. W. Barnes, A survey of Titan's 5-micron-bright terrain, manuscript in preparation, 2007) as it is both the widest spectral window and the one least affected by the atmosphere.

[9] Titan's surface temperature, 93.6 K [*Fulchignoni et al.*, 2005], is low enough that VIMS sees only reflected solar illumination and not thermal emission. VIMS' nominal inherent angular resolution is 0.5 milliradians, and it is 0.25 milliradians in hi-res mode in the sample dimension only; see *Brown et al.* [2004] for a detailed description of how the VIMS instrument operates. We reduce the VIMS data from instrument data numbers into I/F following the procedure described by *Barnes et al.* [2007].

[10] When observing Titan at high phase angles, the scattering of sunlight by atmospheric haze particles contributes a relatively larger fraction of VIMS' detected flux values than does surface reflection. Efforts to develop techniques to deconvolve the atmospheric and surface contributions from VIMS data are ongoing, but yet some time from fruition. Hence in this work we compare spectra of locations on the surface relative to one another, and not in an absolute sense. The color scheme that we employ in the figures follows that of *Barnes et al.* [2007], with red as 5.0 μm, green as 2.0 μm, and blue as 1.28μm. The relative appearance of the dark brown and dark blue surface spectral units is similar to their appearance when using the *Soderblom et al.* [2007a] color scheme.

[11] In this paper we analyze VIMS observations from Cassini's Tb and T9 flybys of Titan (see Figure 1). The Tb data used herein comprise a 2 by 5 mosaic of 80 millisecond exposures covering the middle of Xanadu with a maximum spatial resolution of 6.7 km per pixel.

[12] The T9 flyby was designed with a high closest approach altitude (10400 km) over Titan's equator during which the optical remote sensing instruments, including VIMS, were observing. The hemisphere of Titan facing the spacecraft was lit during ingress; we continued to observe through closest approach and into lookback operations at high emission angles, which were therefore also high phase angles (up to 135 degrees).

2.2. RADAR

[13] Cassini's RADAR operates at a wavelength of 2.2 cm using both passive (radiometry) and active (synthetic aperture, scatterometry, and altimetry) modes [*Elachi et al.*, 2004]. In synthetic aperture radar (SAR) mode, near closest

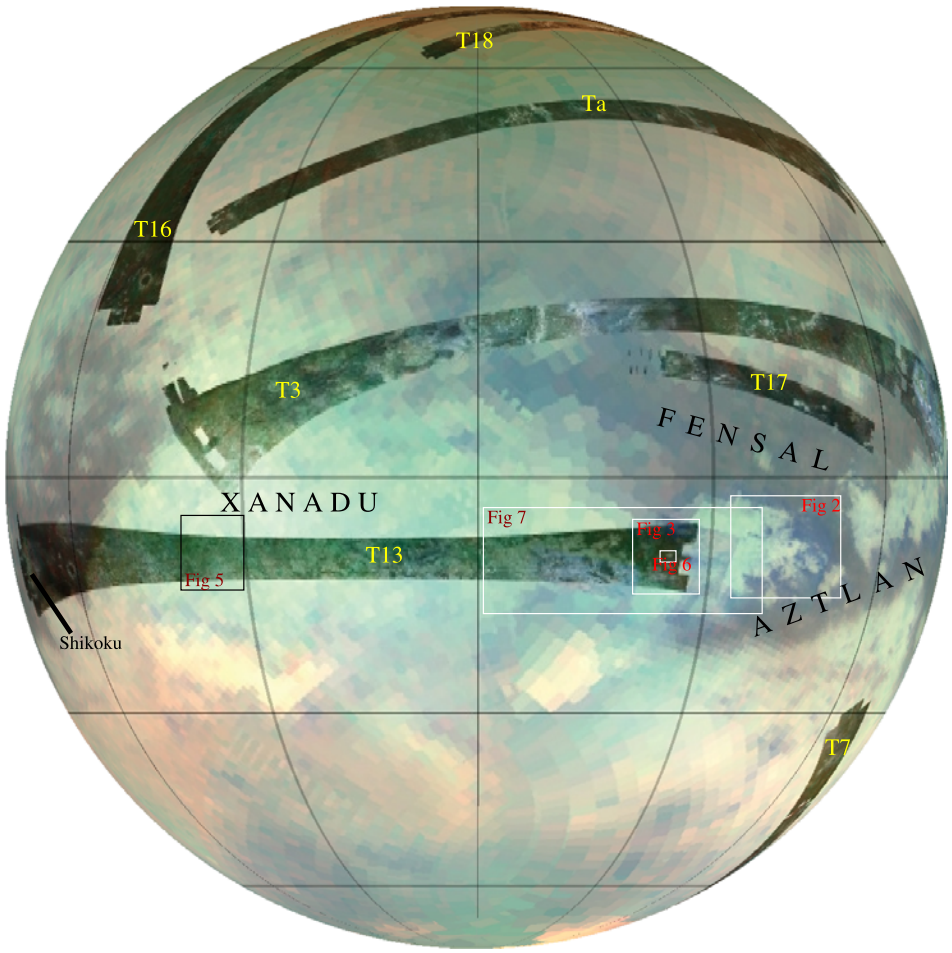

Figure 1. Global combined VIMS/RADAR view of Titan. This figure uses the VIMS basemap from *Barnes et al.* [2007] using data from T8 (28 October 2005) and T9 (26 December 2005) with colors R = 5 μm, G = 2 μm, B = 1.3 μm projected into an orthographic view from above the equator at 90° west longitude. All or part of RADAR SAR swaths Ta (26 October 2004), T3 (15 February 2005), T7 (7 September 2005), T13 (30 April 2006), T16 (22 July 2006), T17 (7 September 2006), and T18 (3 September 2006) are present and shown on this, the leading hemisphere. RADAR views are colored according to the underlying VIMS spectra. The locations and outlines of the areas shown in later Figures 5, 7, 3, 6, and 2 (L to R) are also depicted.

approach to Titan, Cassini produces strips of imaging data thousands of kilometers long and hundreds of kilometers wide with ground resolutions varying from a few hundred meters to ~1 kilometer depending on the spacecraft-target distance [e.g., *Elachi et al.*, 2005]. This paper utilizes data obtained using only the SAR mode.

[14] The intensity of the radar echo from any given point on the surface is a combination of the first-surface reflection (which depends on roughness and the dielectric constant of the surface, and its orientation relative to the beam) and, more important for icy bodies than terrestrial planets, a subsurface or volume-scattering component, which depends on the number density and size of scatterers, the absorptivity of the matrix material, and the dielectric contrast between the matrix and the scatterers. The relative contribution of these factors cannot be determined from a single backscatter measurement but is presently under study for Titan.

[15] As the SAR technique provides its own illumination, it produces images of highest intensity for a backscattering surface and lowest for a forward-scattering one. The surface roughness at the 2.2 cm length scale controls the degree to which the surface backscatters; rougher surfaces are more backscattering, and thus appear brighter in a SAR image. Conversely, surfaces that are smooth at 2.2 cm length scales specularly reflect the incident beam away from the spacecraft, since the incidence angle is ~25° away from the vertical, and thus appear dark.

[16] Variations in the electromagnetic properties of the target material can also affect the net SAR return via volume-scattering. Some of the 2.2 cm wavelength beam reflects off the top surface, but the rest of it continues to propagate into the target. If this penetrating wave encounters additional surfaces, as can exist from subsurface faulting, fracturing, or compositional variations, reflections can result. The depth of penetration for the radar is a function of the material's properties, but is probably between 10s of

centimeters and 10s of meters for the materials Titan. Hence a change in subsurface composition could mimic a change in surface radar return under the right circumstances. Passive microwave radiometry has the potential to address the degeneracy, as it is sensitive to the surface's emissivity.

[17] The position of a feature in the SAR image plane is determined by its azimuth (which determines the component of the Doppler shift due to the observer's motion) and the delay time of the echo. This mapping of cross-track position from time delay assumes a smooth surface (a spherical Titan). Therefore a reflector that is above the reference surface will give an echo with a shorter delay than it would if it were on the reference surface. Thus its inferred position will be closer to the groundtrack than its real location; mountains appear therefore to ''layover'' toward the observer. Symmetric mountains have a characteristic compression on their uprange sides, paired with stretching of the downrange side. Assuming that the mountain lies on a plane of constant elevation, this asymmetry can be used, knowing the observation incidence angle, to infer the height of the mountain. This approach (which can be thought of as image foreshortening) was used to determine a 1300 ± 200 meter depth for the impact crater Sinlap on T3 [*Elachi et al.*, 2006].

[18] A second approach, radarclinometry, relies on the increase of backscatter at lower incidence angles: surfaces tilted toward the radar are brighter. The technique is an analog of photoclinometry, although with two important differences. First, the observation is always at zero phase since the signal is sent from the same location as the receiver. Second, even with a perfect diffuse reflector, i.e., with reflectivity invariant with incidence angle, a radar image will still show uprange slopes as brighter than downrange slopes, because the pixels are defined in range space. There is thus more reflecting surface in a single range pin (pixel) in an uprange slope. The technique, as with photoclinometry, relies on the reflection function being uniform across the scene. The radarclinometric approach, with a characteristic bright-dark pairing in images indicating relief, has been used to detect and measure many topographic structures on Titan, including the dome Ganesa Macula [*Neish et al.*, 2006], the 150 m-high sand dunes [*Lorenz et al.*, 2006], and mountains [*Radebaugh et al.*, 2007].

[19] Synthetic aperture radar data used here come from Cassini's T13 Titan flyby (see Figure 1). Kirk (manuscript in preparation, 2007) described these data. The swath starts just west of Shikoku Facula, reaches its greatest resolution over Xanadu, and extends eastward to near 63 degrees west longitude. SAR illumination is from the north on this right-looking pass. Though the instrument acquired SAR data all the way to near 45 degrees west, this eastward end of the swath was lost due to an error encountered while transmitting these data back to Earth.

2.3. Combining VIMS and RADAR

[20] *Soderblom et al.* [2007a] pioneered study of Titan's surface using the combination of VIMS and RADAR data. Co-located observations from the two instruments have shown that the VIMS' dark-brown spectral unit corresponds to longitudinal dune fields [*Soderblom et al.*, 2007a], allowing global mapping of where dunes probably cover the surface [*Barnes et al.*, 2007].

[21] To register the two data sets, we use the SPICE [*Acton*, 1999] geometric routines to map-project the VIMS observations, but we then register the VIMS data to the RADAR map geometry. RADAR pixel positioning is more accurate because its pixel positioning depends on Doppler and range, and is thus not subject to spacecraft pointing error, as is VIMS. Additionally, as VIMS is a spot-scanner, pointing variations on timescales too short for the SPICE kernels to rectify cause some warping of the map-projection within individual VIMS images, making their rectification less reliable in some cases.

3. Channels

3.1. Description

[22] Branching, dark, curvilinear features are visible in T9 VIMS data (Figure 2 and Figure 3). On the basis of their plan-view morphological similarity to the channels observed in Huygens Descent Imager and Spectral Radiometer (DISR) imagery [*Tomasko et al.*, 2005], RADAR maps (Figure 4) (Lorenz et al., submitted manuscript, 2007), and images from the Imaging Science Subsystem (ISS) [*Porco et al.*, 2005], they were inferred to represent surface runoff channels [*Barnes et al.*, 2007; Clark et al., manuscript in preparation, 2007]. There are two geographically and morphologically distinct sets of channels visible in VIMS imagery (Figure 2). Channels in the south, including those marked A through D, are collectively named Sirith Flumina. A second set of channels oriented radially to a circular blue feature are located in the mid- to northern part of the image.

[23] The southern channels are situated within equatorial bright terrain as described by *Barnes et al.* [2007], adjacent to a boundary within the dark blue terrain [*Soderblom et al.*, 2007a; *Barnes et al.*, 2007]. The channels are more diffuse (less dark) and possibly more numerous in the west. Toward the east, they join or coalesce into darker, fewer channels with distance toward the bright-dark boundary, where they are no longer visible.

[24] On the basis of this network morphology, we infer that the liquid within the southern channels flowed from equatorial bright into the surrounding dark blue terrain, and therefore that the equatorial bright terrain is elevationally above the dark blue unit at this particular location. This result is consistent with DISR observations of the Huygens landing site [*Tomasko et al.*, 2005]. The liquid in the radially oriented channels to the north must have flowed either toward or away from the blue circular feature. The inference from the southern set of channels that the dark blue terrain is lower than the bright terrain suggests that flow was likely inward toward the blue feature.

[25] That VIMS is able to detect the narrow channels at all given the coarse surface spatial resolution (~5 km/pixel) in Figure 2 is perhaps surprising, but it is not uncommon for linear markings of high-contrast that extend over many pixels to be detectable even if their width is smaller than the image resolution [*Schowengerdt*, 1997, p. 70]. Since the channels are not resolved, though, their widths cannot be directly determined from imaging alone in this data set.

[26] In Figure 3, both VIMS and RADAR see the same set of 3 prominent channels oriented radially to Mabon

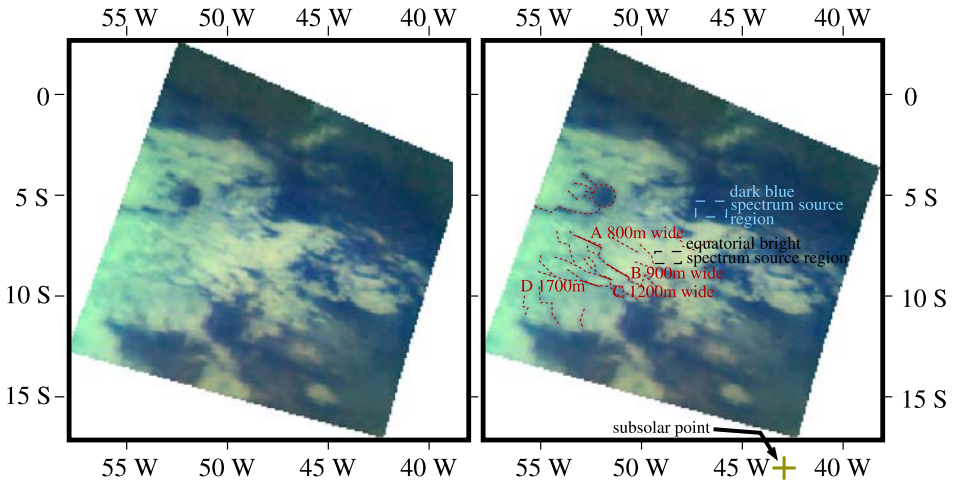

Figure 2. Channels as seen by VIMS during the T9 flyby 26 December 2005. These channels collectively have the proposed name Sirith Flumina. Colors are the same as in Figure 1; contrast has been enhanced. A latitude/longitude grid is shown along the outside for scale; on Titan there are 45 kilometers per degree at the equator. Dashed red lines in the annotated version on the right indicate the interpreted location of channels. Some of the channels drain this equatorial bright region internally into the circular blue feature at 5°S 52°W; the rest drain externally into the surrounding dark blue terrain within Fensal and Aztlan. Although these networks appear rudimentary in comparison with the valley networks revealed by recent Mars research, we think that they compare similarly to the Mariner 9 mapping of fluvial features at similar spatial resolution (1–10 km/pixel) [*Pieri*, 1976]. Spectroscopically measured channel widths averaged along the thick red lines are shown on the right, along with the spectral component areas averaged to determine the widths (see text).

Macula (the radar-rough VIMS-blue feature at the center of the image). Though determination of flow-directions and drainage patterns has been difficult within Xanadu (Kirk, manuscript in preparation, 2007), our wide, areal coverage with both VIMS and RADAR, combined with a fortuitous geometry, give us the opportunity to attempt to interpret the flow directions in this particular area.

[27] West of the area depicted in Figure 3, RADAR imagery shows a distinct lack of channels. Further west, however, more channels appear. We interpret this as a divide, such that the channels on the west and south of Mabon Macula are flowing toward it and the channel to the northeast flows away. The channels' transition, from straighter morphology in the far western and southern reaches to more noticeable meandering and/or braiding closer to Mabon Macula, suggests a transition from steeper to more gently sloping terrain. This is consistent with the interpretation of the western and southern channels flowing from a drainage divide toward Mabon Macula.

[28] The channels described above are not necessarily representative of all of Titan. In particular, the channels surrounding Mabon Macula appear radar-rough, which is not true of many channels viewed by RADAR [*Stofan et al.*, 2007; Lorenz et al., submitted manuscript, 2007]. VIMS coverage of central Xanadu from Tb overlapped with part of the RADAR T13 swath (Figure 5). In the near infrared, Xanadu is characterized by its both relatively high albedo in spectral windows other than 5 microns, and low contrast. The channels in Figure 5 are of lower contrast than Sirith Flumina and the channels around Mabon Macula, though this may be the result of coarser spatial resolution in the VIMS Xanadu data. No distinct channels have been reported within the dark blue and dark brown spectral units, and VIMS resolution to date has been insufficient to discern channels southward of ~35° south latitude.

3.2. Measurement

[29] The spectral character of the channels within equatorial bright terrain matches that of the dark blue spectral unit into which they flow. The dark blue unit shows a spectral signature indicating higher water ice content relative to the rest of Titan [*Rodriguez et al.*, 2006]. The Huygens probe landed on an instance of the dark blue spectral unit [*Soderblom et al.*, 2007a]. The individual VIMS pixels that are on the channels apparently represent a mixture of dark blue and surrounding equatorial bright, as the channels themselves are not spatially resolved.

[30] We therefore attempt to recover the channels' widths on the basis of a best-fit mixing ratio calculated for each pixel. We model each channel-containing pixel as a linear mixture of equatorial bright and dark blue spectra, fitting fill fractions using a least-squares minimization. Then, utilizing the channels' orientations and VIMS' resolution in that dimension and assuming the channel to be linear, we infer the channels' widths that we show in Figure 2b and Figure 3d. The values indicated are heavily dependent on the aforementioned assumptions (i.e., spectral end-members and straight channels) and therefore the numbers may include systematic errors.

[31] Our measured widths for the largest, most easily detected channels vary from ~800 meters to ~2000 meters. These values agree with the values measured by R. Jaumann et al. (Evidence for surface erosion by catastrophic runoff on Titan, submitted to *Icarus*, 2007) of resolved channels

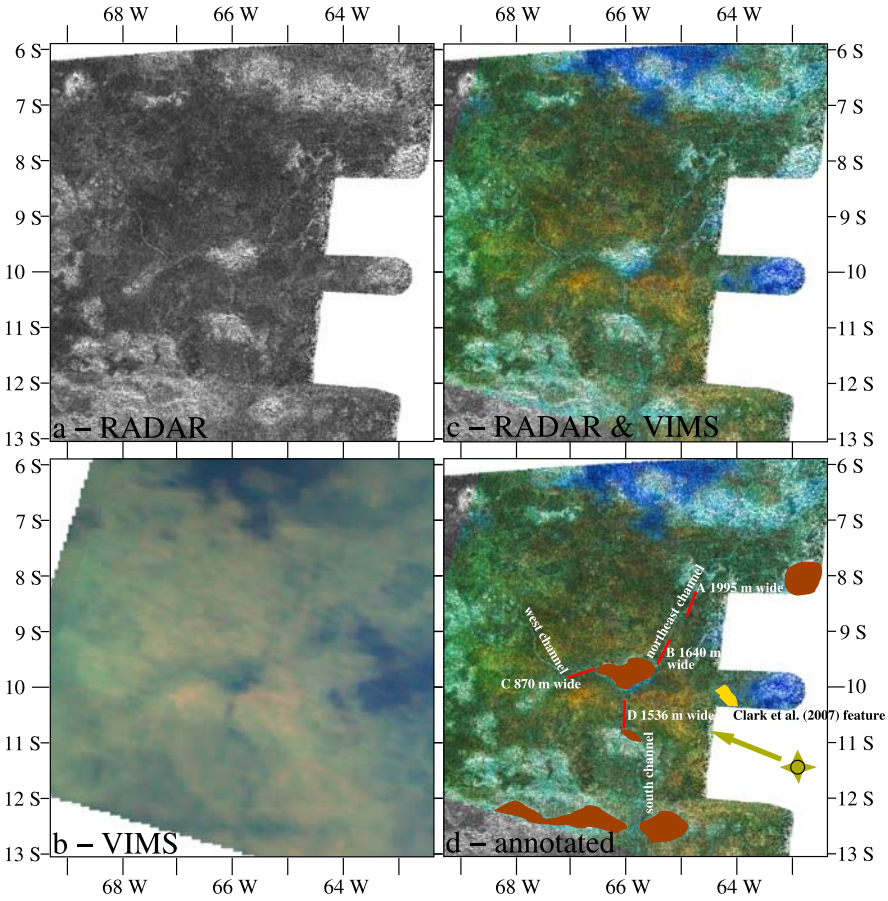

Figure 3. The area at the east end of the RADAR T13 (30 April 2006) swath shown in views from (a) RADAR, (b) VIMS T9, (c) RADAR for value and VIMS for color, and (d) annotated. A latitude/longitude grid is shown along the outside for scale; on Titan there are 45 kilometers per degree at the equator. Unlike within the region surrounding the Huygens landing site [*Soderblom et al.*, 2007a], channels present in the views from both instruments make for strong correlations. The areas painted brown in Figure 3d are ones that show evidence of mountain ranges in RADAR and that appear darker and bluer than their surroundings in the VIMS view. In yellow is a VIMS dark blue/RADAR smooth area located near the interpreted source of windblown material showing an unusually low 2.8/2.7 μm ratio by Clark et al. (manuscript in preparation, 2007). The area shows no easily evident indications of a surface vent in the RADAR view.

using 400-meter resolution VIMS data from the T20 (2006 October 25) flyby. Direct comparison of the VIMS-measured channel widths to those determined by RADAR would be helpful, and we do so using the combination of VIMS T9 (26 December 2005) observations and the eastern end of the T13 (30 April 2006) RADAR swath shown in Figure 3.

[32] Though the channels' locations are suggested from RADAR mapping (such as in Figure 3a), their precise margins are not well defined. In Figure 4 we attempt to delineate possible boundaries for the channels as viewed in RADAR. These boundaries are non-unique, and hence no unambiguous measurement of RADAR channel widths is possible. The SAR imaging and the boundaries we show are, however, consistent with the spectral mixing channel widths described above. The subtle signature also makes radarclinometric measurements impossible, even though qualitatively RADAR glints from the south sides of some channels and dark lanes at the north side indicates that at least some of the channels are incised.

3.3. Discussion

[33] Due to its low reflectivity at 1.6, 2.0, and 5 microns relative to that at 0.94, 1.08, and 1.28 microns, the dark blue spectral unit has been interpreted to represent a composition enhanced in water-ice content relative to the rest of Titan's surface [*Rodriguez et al.*, 2006; *Soderblom et al.*, 2007a; *Barnes et al.*, 2007]. Since the channels surrounding Mabon Macula in Figure 3 are well-modeled as dark blue material surrounded by equatorial bright material, we infer that the channels similarly contain a relative enhancement of water-ice. We note, however, that certain organics or a combination of organics can mimic the water-ice signature; hence although water-ice enhancement seems the most likely explanation, organics cannot at present be ruled out (Clark et al., manuscript in preparation, 2007).

[34] Huygens landed within an outcrop of the dark blue spectral unit and observed channels leading into it from what we now call the equatorial bright unit. Hence the Huygens landing site may be a usable analog for our

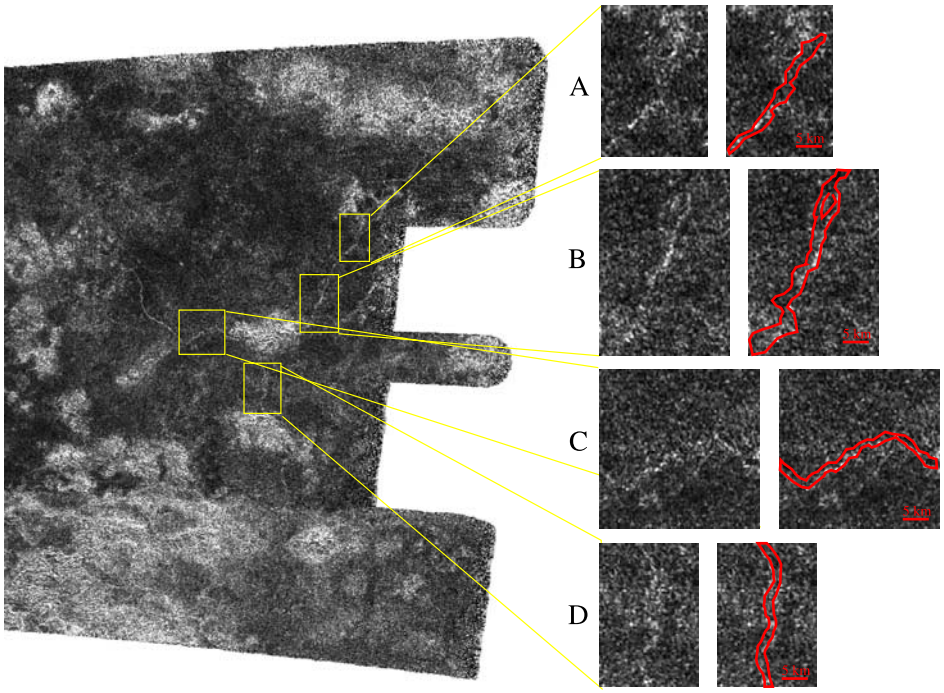

Figure 4. Closeup view of the channel areas for which the spectroscopically measured widths are shown in Figure 3. When viewed in synthetic aperture RADAR, the channel boundaries are not well-defined (Lorenz et al., submitted manuscript, 2007), making direct comparison of channel widths between RADAR and VIMS not as yet possible.

channel observations. The landing site is strewn with rocks 10–15 cm in diameter that are presumably water ice coated with organics [*Tomasko et al.*, 2005]. The rocks are rounded, and thus may have been carried down into the dark blue area by flood- or stream-flow from neighboring channels. RADAR views of the Mabon Macula channels show them in some places to be rough at 2.2 cm and in other places not to be. This could represent a rocky channel-bed composed of rocks varying in diameter along the channel-length.

[35] The Mabon Macula channels are therefore of different composition than the area that they flow through. This is somewhat unexpected from a theoretical standpoint; ostensibly we expect that the rock within the channels should be eroding from the surrounding and/or underlying crust, and as such that it should be of the same composition. As VIMS spectra are diagnostic of only the top few microns of the surface, the bulk of the material making up the rocks in the channels and outside the channels could be the same, with a different veneer.

[36] We suggest several hypotheses for the nature of the discrepancy:

[37] 1. The channels have eroded into strata of differing composition from the surrounding rock.

[38] 2. The channel-bed has acquired a mantling, either via chemical alteration of the host rock or via the acquisition of an external coating.

[39] 3. The surface outside the channels has acquired a mantle that is not present within the channels.

[40] We reject hypothesis 1 as inconsistent with the nature of channels on Earth. Though low-flow channels in high-energy environments can have outcropping bedrock at their bottom, even bedrock channels on Earth can show extensive sediment deposits [*Cenderelli and Cluer*, 1998]. As the process is mechanical, the chemical differences between Titan and Earth are not likely to affect fluvial systems' sediment transport behavior qualitatively (though they will do so quantitatively). We find it unlikely that all or even a significant fraction of such sediment would be derived from a lower stratum of crust being eroded by the streambed. Additionally, if there were such a layer it might be expected to outcrop somewhere, or be revealed in the bottom of Sinlap crater. The only in situ example of dark blue material explored so far (that at the Huygens landing site) was clearly composed of materials, likely stream-deposited, not necessarily related to the underlying bedrock.

[41] A thin coating of haze-derived organics, the methane-soluble portions of which are washed off of surrounding areas and preferentially transported into the channels [e.g., *Smith et al.*, 1996], is one mechanism that could underlie hypothesis 2. The presence elsewhere on Titan of a bright blue spectral unit [*Barnes et al.*, 2006, 2007] implies that, although organics could neutrally darken such a surface, they need not be present for the surface reflectivity to show water-ice characteristics.

[42] *Soderblom et al.* [2007a] suggested that the equatorial bright spectral unit may be covered in an infrared-bright coating of haze-derived nitriles and organics (our hypothesis 3). In this scenario, mechanical or chemical erosion within the channels may strip such a coating off of component rocks, revealing an icier layer below. Water ice is insoluble in liquid methane and ethane. Alternately, the water-ice signature from the VIMS channels could be a result of larger, water-ice-rich sediment remaining as a bedload lag in the channel, whereas the much finer-grained organic sedi-

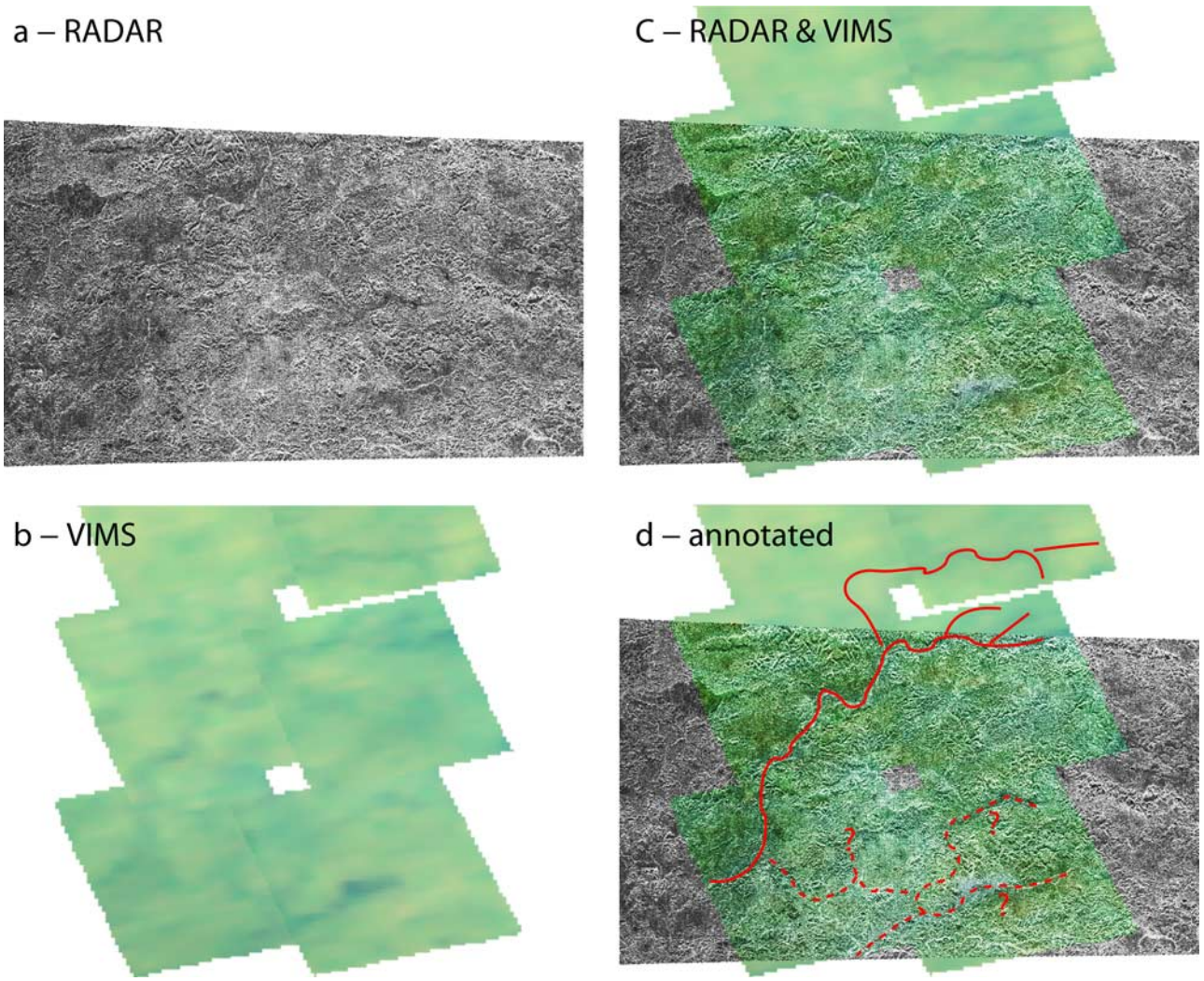

Figure 5. Views of a region near the center of Xanadu as seen from (a) RADAR on T13 (30 April 2006), (b) VIMS on Tb (31 December 2004), (c) RADAR for value and VIMS for color, and (d) annotated). Colors for VIMS are the same as those from Figure 1; contrast has been heavily enhanced. Note the spectral uniformity of this area as compared to Figure 3. The ability to trace channels in the VIMS view outside of the RADAR swath and to verify the existence and locations of the indistinct VIMS channels in the fine-resolution RADAR view should prove valuable for global channel mapping.

ment is flushed through [*Burr et al.*, 2006; *Burr*, 2007]. The possibility of mechanical erosion is suggested by the rounded appearance of the inferred water-ice cobbles coated with organics, observed at the Huygens landing site [*Tomasko et al.*, 2005; *Perron et al.*, 2006], that resemble river cobbles rounded by abrasion during fluvial transport on Earth. This scenario does not necessarily explain the low overall albedo of the channels relative to the bright blue terrain. It is conceivable that larger grains within dark blue terrain relative to bright blue terrain could create the albedo difference.

[43] We suggest that a combination of hypotheses 2 and 3 may be at work. Of the organic haze that settles onto the surface, the soluble portion could be mobilized by methane rainfall and preferentially washed into channels and then out into the dark blue spectral unit. These organics would be dark, accounting for the bright blue and dark blue spectral units. The insoluble portion would then be left behind, coating the surrounding surface, only to be stripped away when those rocks are mechanically mobilized by flowing surface liquid.

[44] Laboratory-measured solubilities of various organic and nitrile solids in liquid methane and ethane may support the idea of solubility-dependent fractionation. Selected solubilities, measured by *Dubouloz et al.* [1989] and shown in Table 1, indicate a range of variation in solubility of three orders of magnitude between various organic species. In general, the solubilities for nitrogen-bearing compounds are lower than those for nitrogen-free organics. The largest solubility is for acetylene, predicted by photochemical models to be the most abundant product of methane stratospheric chemistry after ethane [*Wilson and Atreya*, 2004]. Down by a factor of 500 in predicted net production rate is cyanogen, which has a solubility according to the table somewhere between 400 and 2000 relative to acetylene. Because of this comparable scaling of abundance and

Table 1. Organic and Nitrile Solubilities[a]

Compound	Solubility in Methane-Rich Liquid	Solubility in Ethane-Rich Liquid
Acetylene (C_2H_2)	4×10^{-4}	4×10^{-4}
Propyne (C_3H_4)	3×10^{-5}	5×10^{-5}
Carbon dioxide (CO_2)	3×10^{-6}	1×10^{-5}
Hydrogen cyanide (HCN)	2×10^{-6}	9×10^{-6}
Cyanogen (C_2N_2)	2×10^{-7}	1×10^{-6}

[a]From *Dubouloz et al.* [1989].

solubility, we cannot predict which compounds will tend to come out of solution first. Most likely is that a mixture of hydrocarbon and nitrile precipitates will be present where outflows evaporate.

[45] One interesting uncertainty is the solubility of benzene, which was not reported by *Dubouloz et al.* [1989], and is reported elsewhere in the chemical literature but at temperatures too high to be relevant to the present study [e.g., *Tiffin et al.*, 1979]. Although benzene (C_6H_6) is produced by stratospheric photochemistry at a net rate 1000 times less than that of acetylene, the latter may convert to it and other molecules in exothermic reactions initiated by an appropriate surface catalyst [*Matteson et al.*, 1984]. Cosmic ray irradiation may also trigger explosions of solid organics [*Benit and Roessler*, 1993]. We therefore speculate that the disturbances associated with fluvial flow might convert some acetylene to benzene, and that if the solubility of the latter is substantially less at 95K than that of the former then the product might form a precipitate in the outwash areas. In the absence of laboratory data, the best evidence for this process occurring is the VIMS discovery of absorption bands attributed to benzene that occur preferentially within channels and outwash regions (Clark et al., manuscript in preparation, 2007).

4. Mountains

[46] The VIMS T9/RADAR T13 overlap region contains many mountain ranges as identified by RADAR (Kirk, manuscript in preparation, 2007); this area is the first opportunity to explore for spectral variation in mountains located within the equatorial bright unit. Previous analysis of mountains in VIMS/RADAR overlap areas northwest of Sinlap crater did not show meaningful correlations [*Soderblom et al.*, 2007a].

[47] Surprisingly, RADAR shows the VIMS blue-colored area with channels radial to it (Mabon Macula) to be a mountain range (Figure 6). The topography of this feature is revealed by the bright, linear striations oriented perpendicular to the RADAR illumination direction [see *Radebaugh et al.*, 2007]. Radarclinometry measurements indicate that this range is modest by Titanian standards, with estimated peak heights of ~400 m and overall elevation from valley floor to summit of >1 km.

[48] Mabon Macula and other similarly identified mountain ranges in the overlap region show a spectral character similar to that of the channels, i.e., brighter at 0.94 μm, 1.08 μm, and 1.28 μm than at 1.58 um, 2.0 μm, and 5 μm relative to the rest of Titan. For mountains, very rough topography could itself drive spectral variations through a roughness-dominated phase function [e.g., *Buratti et al.*, 2006] combined with changing illumination conditions as a function of wavelength. When representing directly illuminated rough surfaces at high phase angle, a significant fraction of the surface filling function is composed of shadowed areas, causing the area to appear darker than surrounding terrain of identical spectral reflectivity. On Titan, enhanced atmospheric scattering at shorter wavelengths would fill in the shadows, leading to a relatively blue-appearing surface.

[49] The above arguments notwithstanding, we do not favor the rough phase function/shading scenario for several reasons. First, the low incidence angle across the VIMS scene in Figure 3, 15–25°, ensures that brightness variations resulting from topography would be shading, not shadowing. Scattered light would still fill in the dark shading, but the effect would be lessened. Secondly, the spectral character of mountainous regions matches that of the channels. The channel spectra cannot result from shading because the spectra are the same regardless of channel orientation relative to the local sun direction; that the mountains' spectra match that of the channels implies that the mountains are also not shaded. Lastly, the infrared appearance of RADAR mountains is the same as that of the adjacent rough terrain. That the areas known to have large topographic variation are not spectrally distinct from those merely rough at 2.2 cm scales also argues against the mountains' infrared appearance being the direct result of topography.

[50] We therefore favor the interpretation that the spectral distinctiveness of mountains, as observed in the area east of Xanadu, results from variability in surface properties. Since the mountains' spectra match those of the neighboring channels, the cause of the variations might be similar. Mountains and radar-rough areas might be expected to experience more intense erosion than radar-smooth areas by virtue of their greater exposed surface area. These areas might then either have a thinner or less-complete covering of any haze-derived nitriles and hydrocarbons, leading to their spectral distinctiveness.

[51] Areas identifiable as mountains in the T13 RADAR swath show the same slightly darker and bluer (not a blue slope, but rather brighter at 0.94 μm, 1.08 μm, and 1.28 μm relative to longer wavelengths) spectra in the areas west of Mabon Macula extending toward Xanadu as well as shown in Figure 7. This study area consists entirely of the equatorial bright spectral unit, however, we do not see correlations between RADAR mountains and VIMS spectral variations within Xanadu (see Figure 5 or near Sinlap crater [*Soderblom et al.*, 2007a].

[52] The radarclinometry technique for measuring topography from variations in radar reflectivity relies on the assumption that the inherent electromagnetic properties of the surface to be measured are uniform. If the spectral variations that we have noted in mountainous terrain result from a bulk compositional difference between the mountains and their adjacent valleys, then this fundamental radarclinometric assumption may not be valid. Nevertheless, if the spectral variations result from the presence or absence of a thin coating, then the VIMS observations are consistent with the uniform surface radarclinometry assumption.

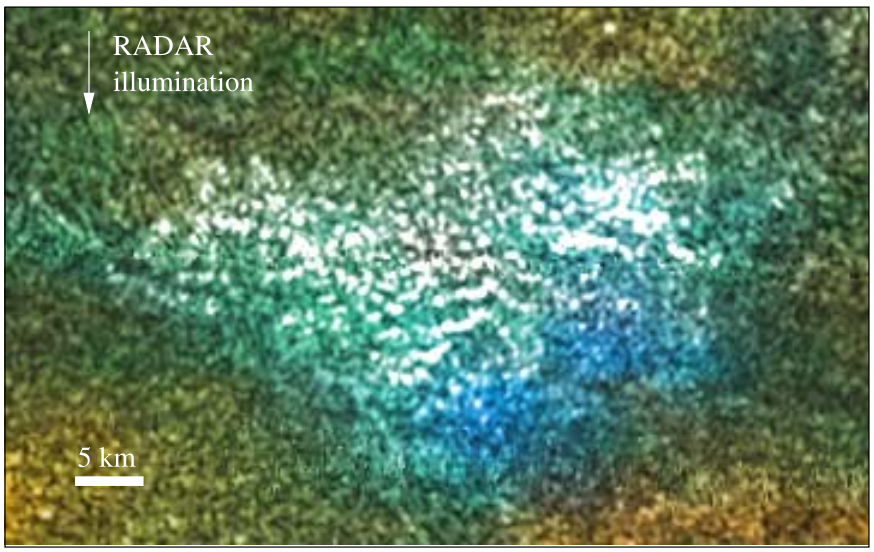

Figure 6. Zoomed view of Mabon Macula, seen at lower zoom at the center of Figures 3 and 4. The linear bright-dark pairs oriented perpendicular to the RADAR look direction are indicative of mountains [*Radebaugh et al.*, 2007].

[53] Huygens observations of drainage patterns near its landing site established that, at that location at least, the darker terrain represents an area of lower elevation [*Tomasko et al.*, 2005]. This observation was used to attempt to ease topographic interpretation of infrared observations [*Rodriguez et al.*, 2006]. Our RADAR/VIMS comparison at Mabon Macula is the first to identify an area that appears darker than its surroundings in near-infrared reflection to stand above those surroundings elevationally. Hence although darker is lower at some bright/dark boundaries as seen in the near infrared, this is not universally the case and future data analysis should be done cautiously in this regard.

[54] We note that in our study area mountains and channels are frequently found in close proximity to one another. A good example of this is near Mabon Macula in Figure 3, where channels from the south and west apparently flow toward and around the mountainous area. While it is beyond the scope of this work to investigate the problem in detail, we suggest a few options as to how this might have come about. (1) The mountains may have formed by block-faulting, resulting in a local topographic low at their base. (2) Isostatic compensation of mountains placed on top of a local plain could lead to a topographically low "moat" surrounding them, similar to the process suggested by *Perron and de Pater* [2004] for Xanadu. (3) The channels may have existed first, and incised as the mountains uplifted (incision rates should be similar to those on Earth [*Collins*, 2005]).

5. Discussion and Conclusion

[55] In investigating the area east of Xanadu that Cassini has observed at fine resolution with both the RADAR and VIMS instruments, we found correlations between mountains and channels between data sets. Channels in this area are perceptible in the VIMS data despite their measured widths (~1 km) being much smaller than the VIMS spatial resolution. The spectral character of the channels matches that of the dark blue spectral unit that the Huygens probe landed on. This unit's spectrum is consistent with a higher water-ice content than the rest of Titan.

[56] The large-scale drainage patterns and flow directions of Titan's channels cannot always be discerned from RADAR mapping alone [Kirk, manuscript in preparation, 2007; Lorenz et al., submitted manuscript, 2007]. The additional coverage provided by VIMS, and the strong contrast of channels as viewed thereby, when combined with fine-spatial-resolution RADAR mapping create a powerful tool. With this tool regional channel-flow and drainage patterns can be mapped so as to delineate large-scale divides and flow sinks. Future work could then eventually decipher topographic gradients to infer global relative topography.

[57] That river channels and dark-blue terrain share spectral qualities implies that they may be causally related. Their relative geographic positions corroborate that relationship. Channels within the equatorial bright unit always empty into the dark blue spectral unit. The dark blue spectral unit, with one exception (Sinlap's ejecta), is located adjacent to equatorial bright terrain and exists preferentially on the equatorial bright unit's eastern margin [*Soderblom et al.*, 2007a; *Barnes et al.*, 2007; *Hayne et al.*, 2006].

[58] We contend that the relative geographic relationship between the equatorial bright, dark blue, and dark brown spectral units derives both from topography and from interplay between sand dune migration and channel outwash (see Figure 8). At the margins of the equatorial bright unit and in the presence of channels, the equatorial bright unit stands topographically higher than the dark blue unit that the channels flow into. Whether dunes (the dark brown spectral unit) or channel outwash (the dark blue spectral unit) dominate in any given area depends on the relative replenishment strength of each.

[59] Near channel mouths, outwash predominates and these areas are covered with the dark blue spectral unit.

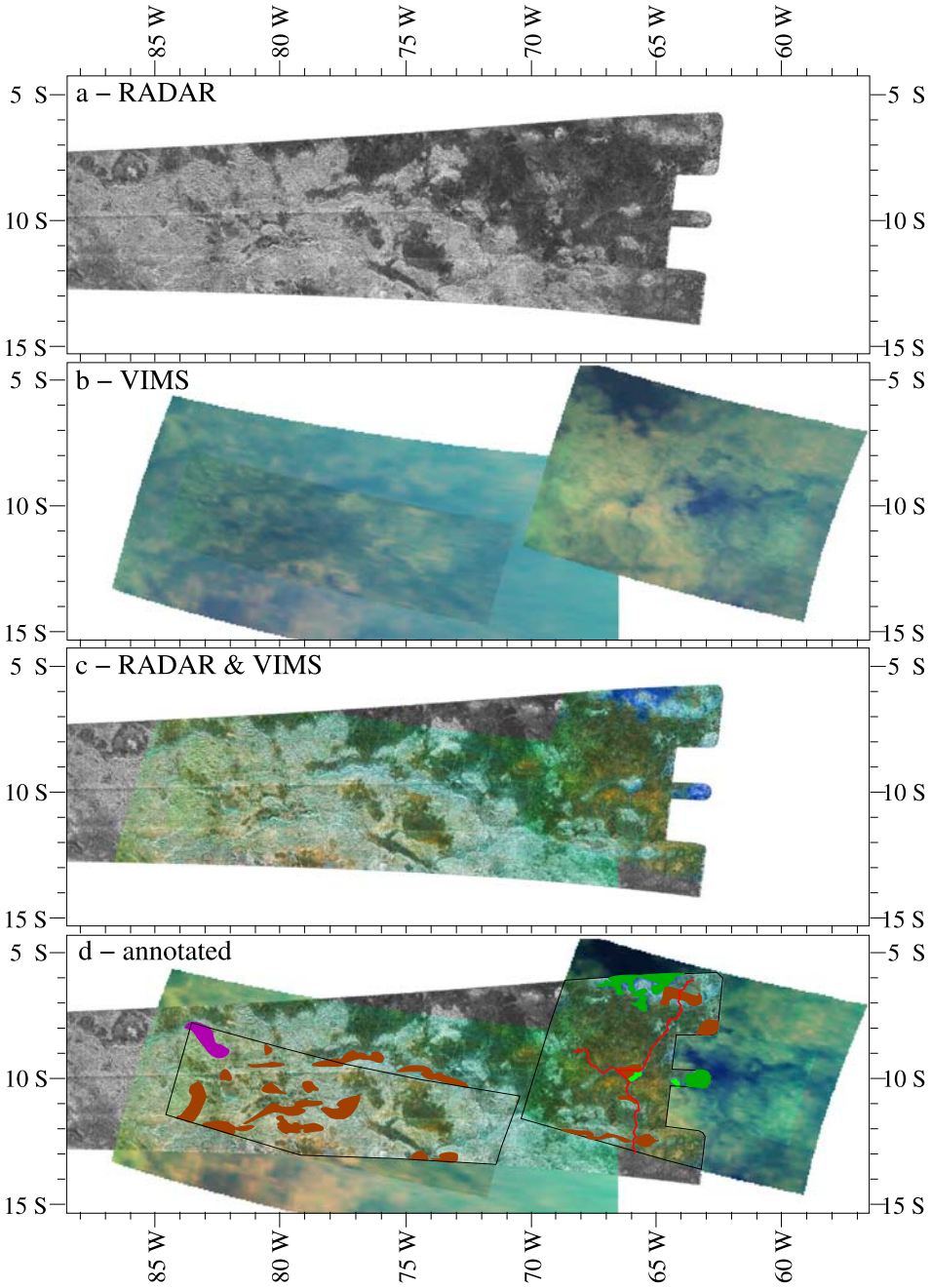

Figure 7. A view of a large portion of the eastern end of the RADAR T13 (30 April 2006) swath shown in (a) RADAR, (b) VIMS, (c) RADAR for value and VIMS for color, and (d) annotated. The VIMS data were obtained during the T9 Titan encounter on 26 December 2005; the subsolar point is the same as that indicated in Figure 2. The eastern VIMS data are the same as those depicted in Figure 3. Those in the west were taken later in the flyby, as the spacecraft was looking back toward Titan's crescent. The phase angle of the western VIMS cubes varies between 80 and 100 degrees, hence the increase in atmospheric scattering relative to the cubes of Mabon Macula taken earlier in the flyby. Brown-painted areas in Figure 7d indicate regions where mountains are indicated by RADAR and that are also bluer and darker than their surroundings as seen by VIMS. Dark green indicates smooth, dark blue areas; red indicates the channels seen surrounding Mabon Macula; and magenta is an area with mountains that does not stand out as distinct from its surroundings in the VIMS view. A latitude/longitude grid is shown along the outside for scale; on Titan there are 45 kilometers per degree at the equator.

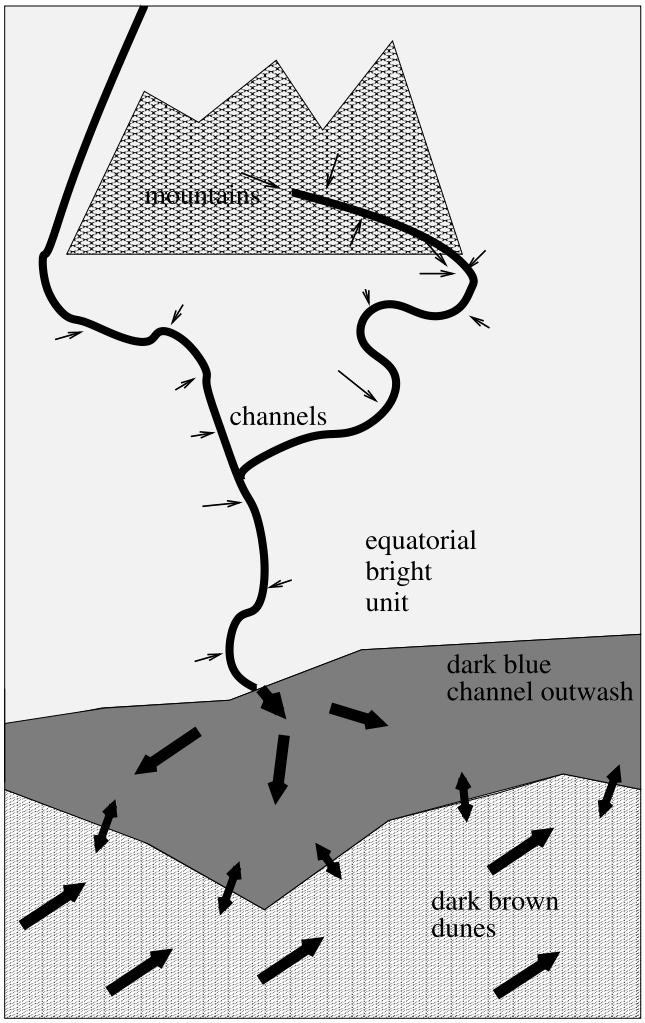

Figure 8. A cartoon model to account for the relative geographic layout of equatorial bright, dark blue, and dark brown spectral units (see section 5). Erosion off of mountains and into channels acquires a dark blue spectral signature (bright at 0.94 μm, 1.08 μm, and 1.28 μm relative to 1.6 μm, 2.0 μm, and 5.0 μm). When the channels reach a low-lying flat area, they dump their washload, creating the terrain we see as the dark blue spectral unit. The outer boundary of the dark blue spectral unit is controlled by an equilibrium between the expansion of outwash area and encroachment by adjacent active dune fields (bottom).

The small, rounded, icy rocks seen on the ground at the Huygens landing site [*Tomasko et al.*, 2005] are consistent with the dark blue spectral unit deriving from channel outwash. Material within Titan's sand dunes is being blown eastward and slightly equatorward on the basis of both sand dune morphology and orientation (J. Radebaugh et al., Dunes on Titan observed by Cassini RADAR, submitted to *Icarus*, 2007) and some circulation models [*Tokano and Neubauer*, 2002]. Hence on the west side of equatorial bright areas, sand covers the ground faster than channel outflow, leaving these areas dark brown. On the north and south sides of equatorial bright terrain, the relative importance of outwash (number and fluence of channels exiting the equatorial bright terrain) and sand dune migration (wind speed and availability of sand upwind) controls whether dark blue or dark brown respectively dominates in these areas.

[60] We also identified that, in our study area east of Xanadu, areas shown to be mountainous by RADAR appear darker and bluer than surrounding terrain when observed by VIMS. We interpret that this spectral variation may result from a thin surficial coating that might be present on the surrounding equatorial bright terrain but either diminished in extent or depth or absent entirely within the mountainous areas. The correlation is present only within equatorial bright terrain, as we do not find it within Xanadu or near Sinlap [*Soderblom et al.*, 2007a].

[61] Near-infrared imaging and spectral mapping complement synthetic aperture radar for studying the surface of Titan. To date there are only a few regions that have been observed at similar spatial resolution with the RADAR and VIMS instruments like the study area east of Xanadu analyzed here. We encourage future overlapping observations with VIMS resolution of 1–5 km/pixel and full RADAR resolution as we think that such observations are likely to reveal further insights than would independent coverage of separate areas.

[62] **Acknowledgments.** J.W.B. is supported by the NASA Postdoctoral Program, administered by Oak Ridge Associated Universities through a contract with NASA, at Ames Research Center. Thanks to NASA and ESA for their support of authors through the Cassini program and the VIMS and RADAR science teams. Thank you to the Cassini RADAR Team for their assistance in and support for the work presented herein.

References

Acton, C. H. (1999), SPICE products available to the planetary science community (abstract), *Proc. Lunar Planet. Sci. Conf.*, *30th*, 1233–1234.

Barnes, J. W., et al. (2005), A 5-micron-bright spot on Titan: Evidence for surface diversity, *Science*, *310*, 92–95, doi:10.1126/science.1117075.

Barnes, J. W., et al. (2006), Cassini observations of flow-like features in western Tui Regio, Titan, *Geophys. Res. Lett.*, *33*, L16204, doi:10.1029/2006GL026843.

Barnes, J. W., et al. (2007), Global-scale surface spectral variations on Titan seen from Cassini/VIMS, *Icarus*, *186*, 242–258, doi:10.1016/j.icarus.2006.08.021.

Benit, J., and K. Roessler (1993), Explosive processes in frozen acetylene irradiated by MeV protons, in *Astronomical Infrared Spectroscopy: Future Observational Directions*, *Astron. Soc. Pac. Conf. Ser.*, vol. 41, edited by S. Kwok, p. 277, Astron. Soc. of the Pac., San Francisco, Calif.

Brown, R. H., et al. (2004), The Cassini Visual And Infrared Mapping Spectrometer (Vims) Investigation, *Space Sci. Rev.*, *115*, 111–168, doi:10.1007/s11214-004-1453-x.

Buratti, B. J., et al. (2006), Titan: Preliminary results on surface properties and photometry from VIMS observations of the early flybys, *Planet. Space Sci.*, *54*, 1498–1509, doi:10.1016/j.pss.2006.06.015.

Burr, D. M. (2007), Comparative sediment transport by flowing liquid on Earth, Mars, and Titan: Synthesis of theory and observations (abstract), *Proc. Lunar Planet. Sci. Conf.*, *38th*, 2222–2223.

Burr, D. M., J. P. Emery, R. D. Lorenz, G. C. Collins, and P. A. Carling (2006), Sediment transport by liquid surficial flow: Application to Titan, *Icarus*, *181*, 235–242, doi:10.1016/j.icarus.2005.11.012.

Cenderelli, D. A., and B. L. Cluer (1998), Depositional processes and sediment supply in resistant-boundary channels: Examples from two case studies, in *Rivers Over Rock: Fluvial Processes in Bedrock Channels*, *Geophys. Monogr. Ser.*, vol. 107, edited by K. Tinkler and E. Wohl, pp. 105–131, AGU, Washington, D. C.

Collins, G. C. (2005), Relative rates of fluvial bedrock incision on Titan and Earth, *Geophys. Res. Lett.*, *32*, L22202, doi:10.1029/2005GL024551.

Coustenis, A., E. Lellouch, J. P. Maillard, and C. P. McKay (1995), Titan's surface: Composition and variability from the near-infrared albedo, *Icarus*, *118*, 87–104, doi:10.1006/icar.1995.1179.

Dubouloz, N., F. Raulin, E. Lellouch, and D. Gautier (1989), Titan's hypothesized ocean properties—The influence of surface temperature and atmo-

spheric composition uncertainties, *Icarus*, *82*, 81–96, doi:10.1016/0019-1035 (89)90025-0.
Elachi, C., et al. (2004), Radar: The Cassini Titan Radar Mapper, *Space Sci. Rev.*, *115*, 71–110, doi:10.1007/s11214-004-1438-9.
Elachi, C., et al. (2005), Cassini radar views the surface of Titan, *Science*, *308*(5724), 970–974.
Elachi, C., et al. (2006), Titan Radar Mapper observations from Cassini's T3 fly-by, *Nature*, *441*, 709–713, doi:10.1038/nature04786.
Fulchignoni, M., et al. (2005), In situ measurements of the physical characteristics of Titan's environment, *Nature*, *438*, 785–791,doi:10.1038/nature04314.
Griffith, C. A., T. Owen, and R. Wagener (1991), Titan's surface and troposphere, investigated with ground-based, near-infrared observations, *Icarus*, *93*, 362–378.
Griffith, C. A., T. Owen, T. R. Geballe, J. Rayner, and P. Rannou (2003), Evidence for the exposure of water ice on Titan's surface, *Science*, *300*, 628–630.
Hayne, P., J. Combe, and T. B. McCord (2006), Omacatl and Elpis Maculae as possible sources of windblown dark material, from Cassini VIMS, *Eos Trans. AGU*, *87*(52), Fall Meet. Suppl., Abstract P13A-0166.
Lopes, R. M.C., et al. (2007), Cryovolcanic features on Titan's surface as revealed by the Cassini Titan Radar Mapper, *Icarus*, *186*, 395–412, doi:10.1016/j.icarus.2006.09.006.
Lorenz, R. D., et al. (2006), The sand seas of Titan: Cassini RADAR observations of longitudinal dunes, *Science*, *312*, 724–727, doi:10.1126/science.1123257.
Lunine, J. I. (1992), Plausible surface models for Titan, in *Proceedings of the Symposium on Titan*, *Eur. Space Agency Spec. Publ.*, *ESA SP*-338, 233–239.
Matteson, D. S., J. I. Lunine, D. J. Stevenson, and Y. L. Yung (1984), Acetylene on Titan, *Science*, *223*, 1131.
McCord, T. B., et al. (2006), Composition of Titan's surface from Cassini VIMS, *Planet. Space Sci.*, *54*, 1524–1539.
Negrão, A., A. Coustenis, E. Lellouch, J.-P. Maillard, P. Rannou, B. Schmitt, C. P. McKay, and V. Boudon (2006), Titan's surface albedo variations over a Titan season from near-infrared CFHT/FTS spectra, *Planet. Space Sci.*, *54*, 1225–1246, doi:10.1016/j.pss.2006.05.031.
Neish, C. D., R. D. Lorenz, P. O'Brien, and T. C. R. Team (2006), The potential for prebiotic chemistry in the possible cryovolcanic dome Ganesa Macula on Titan, *Int. J. Astrobiol.*, *5*, 57–65, doi:10.1017/S1473550406002898.
Perron, J. T., and I. de Pater (2004), Dynamics of an ice continent on Titan, *Geophys. Res. Lett.*, *31*, L17S04, doi:10.1029/2004GL019802.
Perron, J. T., M. P. Lamb, C. D. Koven, I. Y. Fung, E. Yager, and M. dmkovics (2006), Valley formation and methane precipitation rates on Titan, *J. Geophys. Res.*, *111*, E11001, doi:10.1029/2005JE002602.
Pieri, D. (1976), Distribution of small channels on the Martian surface, *Icarus*, *27*, 25–50.
Porco, C. C., et al. (2005), Imaging of Titan from the Cassini spacecraft, *Nature*, *434*, 159–168.
Radebaugh, J., R. D. Lorenz, R. Kirk, J. Lunine, R. Lopes, S. Wall, and R. Team (2007), Mountains on Titan observed by Cassini RADAR, *Icarus*, doi:10.1016/j.icarus.2007.06.020, in press.
Rodriguez, S., et al. (2006), Cassini/VIMS hyperspectral observations of the HUYGENS landing site on Titan, *Planet. Space Sci.*, *54*, 1510–1523.
Schowengerdt, R. A. (1997), *Remote Sensing: Models and Methods for Image Processing*, 2nd ed., Academic, San Diego, Calif.
Smith, P. H., M. T. Lemmon, R. D. Lorenz, L. A. Sromovsky, J. J. Caldwell, and M. D. Allison (1996), Titan's surface, revealed by HST imaging, *Icarus*, *119*, 336–349.
Soderblom, L., et al. (2007a), Correlations between Cassini VIMS spectra and RADAR SAR images: Implications for Titan's surface composition and the character of the Huygens probe landing site, *Planet. Space Sci*, doi:10.1016/j.pss.2007.04.014, in press.
Soderblom, L., et al. (2007b), Topography and geomorphology of the Huygens landing site on Titan, *Planet. Space Sci*, doi:10.1016/j.pss.2007.04.015, in press.
Sotin, C., et al. (2005), Release of volatiles from a possible cryovolcano from near-infrared imaging of Titan, *Nature*, *435*, 786–789, doi:10.1038/nature03596.
Stofan, E. R., et al. (2007), The lakes of Titan, *Nature*, *445*, 61–64, doi:10.1038/nature05438.
Tiffin, D. L., J. P. Kohn, and K. D. Luks (1979), Solid hydrocarbon solubility in liquid methane-ethane mixtures along three-phase solid-liquid-vapor loci, *J. Chem. Eng. Data*, *24*(4), 306–310.
Tokano, T., and F. M. Neubauer (2002), Tidal winds on Titan caused by Saturn, *Icarus*, *158*, 499–515, doi:10.1006/icar.2002.6883.
Tomasko, M. G., et al. (2005), Rain, winds and haze during the Huygens probe's descent to Titan's surface, *Nature*, *438*, 765–778, doi:10.1038/nature04126.
Wilson, E. H., and S. K. Atreya (2004), Current state of modeling the photochemistry of Titan's mutually dependent atmosphere and ionosphere, *J. Geophys. Res.*, *109*, E06002, doi:10.1029/2003JE002181.

K. H. Baines, B. J. Buratti, R. Lopes, K. Mitchell, and S. Wall, Jet Propulsion Laboratory, California Institute of Technology, Pasadena, CA 91109, USA.
J. W. Barnes, R. H. Brown, and J. Lunine, Lunar and Planetary Laboratory, University of Arizona, 1629 East University Boulevard, Tucson, AZ 85721, USA. (jbarnes@lpl.arizona.edu)
D. Burr, Carl Sagan Center, SETI Institute, Mountain View, CA 94043, USA.
R. Clark, U.S. Geological Survey, Denver, CO 80225, USA.
R. Jaumann, DLR, Institute for Planetary Research, Rutherfordstrasse 2, D-12489 Berlin, Germany.
R. L. Kirk and L. Soderblom, U.S. Geological Survey, Flagstaff, AZ 86001, USA.
S. Le Mouélic and C. Sotin, Laboratoire de Planétologie et Géodynamique, UMR CNRS 6112, Université de Nantes, Nantes, France.
R. D. Lorenz, Space Department, JHU Applied Physics Laboratory, Laurel, MD 20723-6099, USA.
P. D. Nicholson, Astronomy Department, Cornell University, Ithaca, NY 14853, USA.
J. Radebaugh, Department of Geological Sciences, Brigham Young University, Provo, UT 84502, USA.
S. Rodriguez, Laboratoire AIM, Centre d'Ètude de Saclay, DAPNIA/Sap, Centre de l'Orme des Merisiers, Bâtiment 709, F-91191 Gif sur Yvette Cedex, France.
C. A. Wood, Planetary Science Institute, Tucson, AZ 85719, USA.